

Article

Radiative MHD Nanofluid Flow over a Moving Thin Needle with Entropy Generation in a Porous Medium with Dust Particles and Hall Current

Iskander Tlili ^{1,2}, Muhammad Ramzan ^{3,*}, Seifedine Kadry ⁴, Hyun-Woo Kim ⁵ and Yunyoung Nam ^{6,*} 

¹ Department for Management of Science and Technology Development, Ton Duc Thang University, Ho Chi Minh City 758307, Vietnam; iskander.tlili@tdtu.edu.vn

² Faculty of Applied Sciences, Ton Duc Thang University, Ho Chi Minh City 758307, Vietnam

³ Department of Computer Science, Bahria University, Islamabad Campus, Islamabad 44000, Pakistan

⁴ Department of Mathematics and Computer Science, Faculty of Science, Beirut Arab University, Beirut 115020, Lebanon; s.kadry@bau.edu.lb

⁵ Department of ICT Convergence Rehabilitation Engineering, Soonchunhyang University, Asan 31538, Korea; lovekhw@gmail.com

⁶ Department of Computer Science and Engineering, Soonchunhyang University, Asan 31538, Korea

* Correspondence: mramzan@bahria.edu.pk (M.R.); ynam@sch.ac.kr (Y.N.)

Received: 5 February 2020; Accepted: 9 March 2020; Published: 18 March 2020



Abstract: This paper investigated the behavior of the two-dimensional magnetohydrodynamics (MHD) nanofluid flow of water-based suspended carbon nanotubes (CNTs) with entropy generation and nonlinear thermal radiation in a Darcy–Forchheimer porous medium over a moving horizontal thin needle. The study also incorporated the effects of Hall current, magnetohydrodynamics, and viscous dissipation on dust particles. The said flow model was described using high order partial differential equations. An appropriate set of transformations was used to reduce the order of these equations. The reduced system was then solved by using a MATLAB tool bvp4c. The results obtained were compared with the existing literature, and excellent harmony was achieved in this regard. The results were presented using graphs and tables with coherent discussion. It was comprehended that Hall current parameter intensified the velocity profiles for both CNTs. Furthermore, it was perceived that the Bejan number boosted for higher values of Darcy–Forchheimer number.

Keywords: entropy generation; nonlinear thermal radiation; energy conservation; magnetohydrodynamic; nanofluid; thin needle

1. Introduction

The novel idea to reduce entropy generation in heat transfer convective processes was floated by Bejan [1]. In thermodynamic systems, this notion is employed to enhance the efficiency of thermal engineering gadgets [2]. Indeed, entropy generation is used to gauge the molecular chaos or disorder in a thermodynamic system. Thermodynamics' second law states that higher molecular disorder is inversely proportional to the quality of energy reduction. It has been examined that energy dissipation and heat transfer owing to differences in temperatures are the key factors for entropy generation. That is why special attention is given for the enhancement of heat transfer in varied engineering applications. The average internal heat loss because of entropy generation in a titanium dioxide (TiO₂) suspended in a water-based nanofluid Poiseuille flow with the impact of mixed convection and thermal radiation in a wavy channel is discussed by Zeeshan et al. [3]. The 2nd law of thermodynamics is betrothed for the entropy generation model erection. It is reported that the pressure gradient is the key factor for a rise

in the average energy loss. Further, it is noted that the entropy generation for the radiation parameter is more near walls in comparison to the middle of the channel. The study of entropy generation in the nanofluid thin-film flow, containing a suspension of both types of carbon nanotubes (CNTs) with Cattaneo-Christov heat flux, magnetohydrodynamics, and variable source/sink, is studied by Lu et al. [4]. Numerical simulations with the erected mathematical model are found by the `bvp4c` function of MATLAB software (University of New Mexico, New Mexico). It is witnessed that entropy generation is larger for higher estimates of the magnetic parameter for a thin film flow. The entropy generation analysis during the heat transfer process in the flow of Ferrofluid with low oscillating magnetic field past a stretched rotating disk is deliberated by Hassan et al. [5]. The analytical solution of the problem is attained via Mathematica-based `bvp 2.0` based on the homotopy analysis method. It is comprehended that total entropy is boosted with the dispersion of nanoparticles. Further, it is noted that the irreversibility of the fluid flow is enhanced by the strong magnetic impact. Some recent literature about entropy generation may be found in references [6–10].

CNTs are cylindrical type carbon allotropes. These were first exposed in the form of multi-walled carbon nanotubes (MWCNTs) by Iijima [11] in 1991. This was followed by another study by Bethune et al. [12] who introduced the idea of single-walled carbon nanotubes (SWCNTs) in 1993. In today's era, a good number of applications involving CNTs may be found, like in health care, energy, electronics, etc. [13–15]. It is now a well-established theory that snags with the materials possessing low thermal conductivity are removed with the introduction of nanofluids. Nanofluids holds nanoparticles with a size of <100 nm. These nanoparticles are made up of copper, metal oxides, alumina, nanomaterials, nitrides, and carbides [16]. The concept of nanofluids was the first time floated by Choi and Eastman [17]. A substantial number of studies have been carried out since its inception [18–20]. Recently, Sheikholeslami and Shehzad [21] numerically examined the flow of nanofluid comprising $\text{Fe}_3\text{O}_4\text{-H}_2\text{O}$ solution in a permeable cavity under the influence of a variable magnetic field using Control Volume Finite Element Method (CVFEM). They observed the highest heat transfer rate in the case of the platelet-shaped nanoparticles. It was further witnessed by them that the velocity of the nanofluid was on the decline once the strong magnetic field was applied. Entropy optimization for the flow of Carreau nanofluid flow with cubic auto-catalysis chemical reaction was studied by Khan et al. [22] analytically. They noticed that the sturdier magnetic field boosted the entropy generation. Sheikholeslami [23] found a numerical solution of nanofluid flow under the influence of the magnetic field in a permeable medium via the CVFEM scheme. He analyzed the influences of entropy and exergy on the presented model and reported that entropy loss enhanced in attendance of stronger magnetic field. Khan et al. [24] examined the numerical solution of 3D cross nanofluid with activation energy and binary chemical reaction with zero mass flux and convective boundary conditions. They noticed that higher estimates of activation energy boosted the concentration of the cross nanofluid. Hosseini and Sheikholeslami [25] analyzed the thermal competence of a convective nanofluid flow with entropy generation inside a microchannel under the influence of the magnetic field. Between two phases, non-equilibrium condition for a permeable media is engaged. They noticed that the entropy generation enhanced with an increase in fluid friction irreversibility. Some recent studies have also highlighted the concept of carbon nanotubes [26–33] and many therein.

Abundant applications focusing on Cattaneo-Christov heat flux amalgamated with thermal radiation may be found in missiles, air crafts, nuclear power plants, space vehicles' propulsion gadgets, etc. Keeping in view these interesting applications, scientists and researchers [34–40] are motivated to look for fluid behavior in attendance of thermal radiation and Cattaneo-Christov heat flux.

Motivated from the above literature, our objective was to find the water-based CNTs dusty nanofluid flow over a moving thin needle. The analysis was performed in the presence of Hall current and nonlinear thermal radiation in a Darcy–Forchheimer porous media. The thermal efficacy of the system was analyzed by employing entropy analysis. A numerical solution of the envisaged inimitable mathematical model was found. To our information, no such study has been conducted so far in the literature. This model was unique in its category. Endorsement of the outcomes of the existing study

was done by comparing with a published article in limiting case. Graphical sketches and tables were also part of this study.

2. Mathematical Modeling

Let us assume an H₂O-CNTs-based nanofluid flow with Hall current over a moving slender needle having speed u_w and radius “ a ” (Figure 1). The speed of fluid far away from the surface is taken as u_∞ . The cylindrical coordinates (x, r) are taken in such a way that x – is along the axis of the needle and r – normal to the axis. The flow containing dust particles is generated in a non-Darcy absorbent media. The associated impacts affecting the flow in the heat equation are viscous dissipation and nonlinear thermal radiation. Furthermore, T_w and T_∞ are the constant temperatures at the wall and far off from the wall with $T_\infty > T_w$. A magnetic field with magnetic strength B_0 is applied with the low Reynold number assumption [41], which eventually results in the induced magnetic field to be neglected. Two types of the equations, i.e., fluid phase and particle phase, comprising the envisioned mathematical model fulfilling laws of conservation are also laid down as given below:

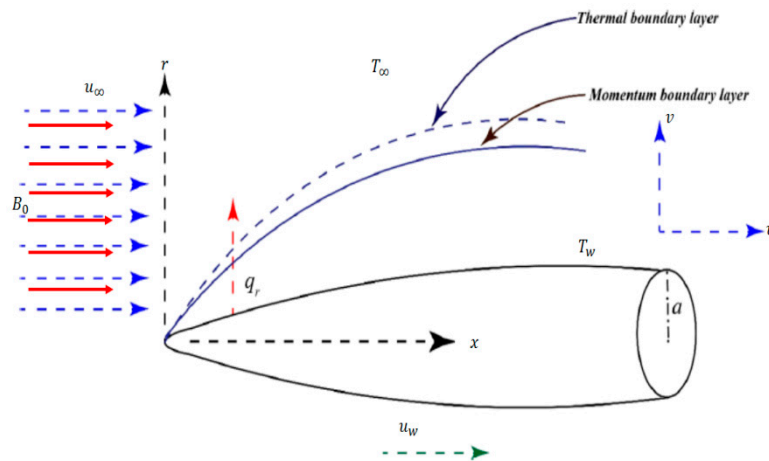


Figure 1. The physical design of the flow problem.

The above flow theory gives rise to the following boundary layer equations [41–45]:

Continuity equation: Fluid phase

$$\frac{\partial(ru)}{\partial x} + \frac{\partial(rv)}{\partial r} = 0, \tag{1}$$

Momentum equation: Fluid phase

$$(1 - \phi_d)\left(u\frac{\partial u}{\partial x} + v\frac{\partial u}{\partial r}\right) = (1 - \phi_d)\left(\frac{\mu_{nf}}{\rho_{nf}}\frac{1}{r}\frac{\partial}{\partial r}\left(r\frac{\partial u}{\partial r}\right)\right) - \frac{\nu_{nf}}{k^*}u - \frac{C_b}{x\sqrt{k^*}}u^2 + \frac{KN}{\rho_{nf}}(u_p - u) - \frac{\sigma B_0^2}{\rho_{nf}(1+m^2)}u, \tag{2}$$

Continuity equation: Particle phase

$$\frac{\partial(ru_p)}{\partial x} + \frac{\partial(rv_p)}{\partial r} = 0, \tag{3}$$

Momentum equation: Particle phase

$$u_p\frac{\partial u_p}{\partial x} + v_p\frac{\partial u_p}{\partial r} = \frac{K}{m_d}(u - u_p), \tag{4}$$

Energy equation: Fluid phase

$$\begin{aligned}
 u \frac{\partial T}{\partial x} + v \frac{\partial T}{\partial r} &= \frac{k_{nf}}{(\rho C_p)_{nf}} \frac{1}{r} \frac{\partial}{\partial r} \left(r \frac{\partial T}{\partial r} \right) - \frac{1}{(\rho C_p)_{nf}} \frac{\partial q_r}{\partial r} + \frac{\mu_{nf}}{(\rho C_p)_{nf}} \left(\frac{\partial u}{\partial r} \right)^2 \\
 &+ \frac{\mu_{nf}}{k^* (\rho C_p)_{nf}} u^2 + \frac{N_1}{\tau_v (\rho C_p)_{nf}} (u_p - u)^2 + \frac{N_1 (C_p)_{nf}}{\tau_T (\rho C_p)_{nf}} (T_p - T) \\
 &+ \frac{\sigma B_0^2}{(\rho C_p)_{nf} (1+m^2)} u^2,
 \end{aligned}
 \tag{5}$$

Energy equation: Particle phase

$$N_1 c_m \left(u_p \frac{\partial T_p}{\partial x} + v_p \frac{\partial T_p}{\partial r} \right) = \frac{N_1 (C_p)_{nf}}{\tau_T} (T_p - T),
 \tag{6}$$

with the boundary conditions

$$\begin{aligned}
 u(x, r) = u_w, \quad v(x, r) = 0, \quad u_p(x, r) = u_w, \quad v_p(x, r) = 0, \\
 T(x, r) = T_w, \quad \text{at } r = R(x),
 \end{aligned}
 \tag{7}$$

$$u(x, r) \rightarrow u_\infty, \quad T(x, r) \rightarrow T_\infty, \quad T_p(x, r) \rightarrow T_\infty \text{ as } r \rightarrow \infty.
 \tag{8}$$

The heat flux in simplified form after considering Rosseland approximation is:

$$q_r = -\frac{4\sigma_{SB}}{3a_r} \frac{\partial T^4}{\partial r},
 \tag{9}$$

where a_r is the mean absorption coefficient, and σ_{SB} is the Stephen–Boltzman constant. For a planer boundary layer flow, the above equation can be written as:

$$q_r = -\frac{16\sigma_{SB}}{3a_r} T^3 \frac{\partial T}{\partial r}.
 \tag{10}$$

The mathematical model proposed by Xue [46] for the CNTs is given in Table 1. The thermo-physical traits of the CNTs of both types and H₂O are appended in Table 2.

Table 1. Properties of the nanofluid defined for the presented model [46].

Properties	Nano-Fluid
Density	$\rho_{nf} = (1 - \phi)\rho_{bf} + \phi\rho_{CNT}$
Heat capacity	$(\rho C_p)_{nf} = (1 - \phi)(\rho C_p)_{bf} + \phi(\rho C_p)_{CNT}$
Viscosity	$\mu_{nf} = \frac{\mu_{bf}}{(1-\phi)^{2.5}}$
Thermal conductivity	$\frac{k_{nf}}{k_{bf}} = \frac{(1-\phi) + 2\phi \left(\frac{k_{CNT}}{k_{CNT} - k_{bf}} \right) \ln \left(\frac{k_{CNT} + k_{bf}}{2k_{bf}} \right)}{(1-\phi) + 2\phi \left(\frac{k_{bf}}{k_{CNT} - k_{bf}} \right) \ln \left(\frac{k_{CNT} + k_{bf}}{2k_{bf}} \right)}$

Table 2. Thermo-physical features of the base fluid H₂O and CNTs [46].

Thermo-Physical Properties	H ₂ O	SWCNT	MWCNT
C_p (j/kgK)	4179	425	796
ρ (kg/m ³)	997.1	2600	1600
k (W/mK)	0.613	6600	3000
Prandtl number (Pr)	6.8	–	–

3. Similarity Transformation

The similarity variables are introduced as follows,

$$\begin{aligned} u &= 2Ug'(\xi), & u_p &= 2UG'(\xi), & v &= \frac{Ur}{x}g'(\xi) - \frac{v_{bf}}{r}g(\xi), \\ v_p &= \frac{Ur}{x}G'(\xi) - \frac{v_{bf}}{r}G(\xi), & \xi &= \frac{Ur^2}{v_{bf}x}, & \theta(\xi) &= \frac{T-T_\infty}{T_w-T_\infty}, & \theta_p(\xi) &= \frac{T_p-T_\infty}{T_w-T_\infty}. \end{aligned} \quad (11)$$

The resulting non-dimensional Ordinary differential equations (ODEs) system after referring to similarity variables:

Momentum equation: Fluid phase

$$\begin{aligned} (1-\phi_d)(1-\phi)^{2.5} &\left(1-\phi+\phi\frac{\rho_{CNT}}{\rho_{bf}}\right)gg''+2(g''+\xi g''')-\lambda g' \\ &-(1-\phi)^{2.5}\left(1-\phi+\phi\frac{\rho_{CNT}}{\rho_{bf}}\right)F_r g'^2+(1-\phi)^{2.5}\alpha\beta(G'-g') \\ &-(1-\phi)^{2.5}\frac{M}{1+m^2}g'=0, \end{aligned} \quad (12)$$

Momentum equation: Particle phase

$$G''G+\beta(g'-G')=0, \quad (13)$$

Energy equation: Fluid phase

$$\begin{aligned} \frac{k_{nf}}{k_{bf}}(\xi\theta''+\theta') &+0.5Pr\left(1-\phi+\phi\frac{(\rho C_p)_{CNT}}{(\rho C_p)_{bf}}\right)g\theta' \\ &+\frac{4}{3N_r}(1+(\theta_r-1)\theta)^2\{3\xi(\theta_r-1)\theta'^2 \\ &+(1+(\theta_r-1)\theta)(0.5\theta'+\xi\theta'')\}+\frac{4EcPr}{(1-\phi)^{2.5}}\xi g''^2 \\ &+2\alpha\beta EcPr(G'-g')^2+2EcPr\left(\frac{\lambda}{(1-\phi)^{2.5}}+\frac{M}{1+m^2}\right)g'^2 \\ &+0.5\alpha\beta_T Pr\left(1-\phi+\phi\frac{(C_p)_{CNT}}{(C_p)_{bf}}\right)(\theta_p-\theta)=0, \end{aligned} \quad (14)$$

Energy equation: Particle phase

$$G\theta'_p-\gamma\beta_T\left(1-\phi+\phi\frac{(C_p)_{CNT}}{(C_p)_{bf}}\right)(\theta_p-\theta)=0, \quad (15)$$

associated with boundary conditions

$$\begin{aligned} g(a) &= \frac{a}{2}\varepsilon, & g'(a) &= \frac{\varepsilon}{2}, & G(a) &= \frac{a}{2}\varepsilon, & G'(a) &= \frac{\varepsilon}{2}, & \theta(a) &= 1, \\ g'(\infty) &\rightarrow \frac{1-\varepsilon}{2}, & \theta(\infty) &\rightarrow 0, & \theta_p(\infty) &\rightarrow 0. \end{aligned} \quad (16)$$

Here, prime represents derivative with respect to ξ . The dimensionless physical parameters are defined as follows:

$$\begin{aligned} \lambda &= \frac{v_{bf}}{2Uk^*}, & F_r &= \frac{C_b}{\sqrt{k^*}}, & \alpha &= \frac{Nm_d}{\rho_{bf}}, & \beta &= \frac{K}{2Um_d}, & M &= \frac{\sigma B_0^2}{2U\rho_{bf}}, \\ Pr &= \frac{v_{bf}}{k_{bf}}(\rho C_p)_{bf}, & N_r &= \frac{a_r k_{bf}}{4\sigma_{SB}T_\infty^3}, & \theta_r &= \frac{T_w}{T_\infty}, & Ec &= \frac{U^2}{(T_w-T_\infty)(C_p)_{bf}}, \\ \beta_T &= \frac{1}{2U\tau_T}, & \gamma &= \frac{(C_p)_{bf}}{c_m}. \end{aligned} \quad (17)$$

4. Nusselt Number and Skin Friction Coefficient

The skin friction coefficients C_{fx} and the local Nusselt number Nu_x in dimensional form are given by:

$$C_{fx} = \frac{2\tau_w}{\rho_{bf}U^2}, \quad Nu_x = \frac{xq_w}{k_{bf}(T_w - T_\infty)}, \quad (18)$$

where τ_w and q_w are defined as below:

$$\tau_w = [\mu_{nf} \frac{\partial u}{\partial r}]_{r=a}, \quad q_w = -k_{nf} \left(\frac{\partial T}{\partial r} \right)_{r=a} + (q_r)_{r=a}. \quad (19)$$

By using Equations (11), (18) and (19) we get

$$\sqrt{Re_x} C_{fx} = \frac{8a^{1/2} g''(a)}{(1-\phi)^{2.5}}, \quad (20)$$

$$\frac{Nu_x}{\sqrt{Re_x}} = -2a^{1/2} \left(\frac{k_{nf}}{k_{bf}} \right) \left(1 + \frac{4}{3N_r} \theta_r^3 \right) \theta'^{(a)}. \quad (21)$$

with

$$Re_x = \frac{Ux}{\nu_{bf}}. \quad (22)$$

5. Entropy Generation

Entropy generation analysis is much important to study the thermal energy irreversibility of a particular system.

$$\dot{S}'''_{GEN} = \underbrace{\left[\begin{array}{l} \frac{k_{nf}}{T^2} \left(\frac{\partial T}{\partial r} \right)^2 + \frac{k_{nf}}{T^2} \left\{ \frac{16\sigma_{SB}}{3a_r k_{bf}} T^3 \left(\frac{\partial T}{\partial r} \right)^2 \right\} \\ \text{Entropy due to heat transfer} \\ \frac{\mu_{nf}}{T^2} u^2 + \frac{\mu_{nf}}{T} \left(\frac{\partial T}{\partial r} \right)^2 \\ \text{Energy due to fluid friction} \end{array} \right]} + \underbrace{\left[\frac{\sigma_{B_0}^2}{T(1+m^2)} u^2 \right]}_{\text{Energy due to diffusion}}, \quad (23)$$

Equation (23), after employing Equation (11), in dimensionless form is

$$N_S = \frac{k_{nf}}{k_{bf}} \xi (\theta_r - 1)^2 \theta'^2 \left(\frac{1}{(1+(\theta_r-1)\theta)^2} + \frac{4}{3N_r} (1 + (\theta_r - 1)\theta) \right) + \frac{4EcPr(\theta_r-1)}{(1-\phi)^{2.5}(1+(\theta_r-1)\theta)} \xi g''^2 + \frac{2EcPr(\theta_r-1)}{(1+(\theta_r-1)\theta)} \left(\frac{\lambda}{(1-\phi)^{2.5}} + \frac{M}{1+m^2} \right) g'^2. \quad (24)$$

Here, the characteristic entropy generation is given by:

$$(\dot{S}'''_{GEN})_0 = \frac{4k_{bf}U}{\nu_{bf}x}, \quad (25)$$

In non-dimensional form, heat transfer irreversibility is given by:

$$N_{HT} = \frac{k_{nf}}{k_{bf}} \xi (\theta_r - 1)^2 \theta'^2 \left(\frac{1}{(1 + (\theta_r - 1)\theta)^2} + \frac{4}{3N_r} (1 + (\theta_r - 1)\theta) \right). \quad (26)$$

The fluid friction irreversibility is defined by:

$$N_{FF} = \frac{4EcPr(\theta_r - 1)}{(1 - \phi)^{2.5}(1 + (\theta_r - 1)\theta)} \xi g''^2, \tag{27}$$

and the porous medium and magnetic field irreversibility are represented by:

$$N_{PMF} \frac{2EcPr(\theta_r - 1)}{(1 + (\theta_r - 1)\theta)} \left(\frac{\lambda}{(1 - \phi)^{2.5}} + \frac{M}{1 + m^2} \right) g'r^2, \tag{28}$$

The Bejan number *Be* in dimensional form is defined as:

$$Be = \frac{\frac{k_{nf}}{T^2} \left(\frac{\partial T}{\partial r} \right)^2 + \frac{k_{nf}}{T^2} \left\{ \frac{16\sigma_{SB}}{3a_r k_{bf}} T^3 \left(\frac{\partial T}{\partial r} \right)^2 \right\}}{\frac{k_{nf}}{T^2} \left(\frac{\partial T}{\partial r} \right)^2 + \frac{k_{nf}}{T^2} \left\{ \frac{16\sigma_{SB}}{3a_r k_{bf}} T^3 \left(\frac{\partial T}{\partial r} \right)^2 \right\} + \frac{\mu_{nf}}{Tk^*} u^2 + \frac{\mu_{nf}}{T} \left(\frac{\partial T}{\partial r} \right)^2 + \frac{\sigma B_0^2}{T(1+m^2)} u^2}. \tag{29}$$

In dimensionless form, *Be* after consulting (11) is:

$$Be = \frac{\left(\xi(\theta_r - 1)^2 \theta r^2 \left(\frac{3N_r}{+4(1 + (\theta_r - 1)\theta)^3} \right) \right)}{\left(\begin{array}{l} \xi(\theta_r - 1)^2 \theta r^2 (3N_r + 4(1 + (\theta_r - 1)\theta)^3) \\ + \frac{12N_r EcPr(\theta_r - 1)}{\left(\frac{k_{nf}}{k_{bf}}\right)(1 - \phi)^{2.5}} \xi(1 + (\theta_r - 1)\theta) g''^2 \\ + \frac{6N_r EcPr(\theta_r - 1)}{\left(\frac{k_{nf}}{k_{bf}}\right)} (1 + (\theta_r - 1)\theta) \left(\frac{\lambda}{(1 - \phi)^{2.5}} + \frac{M}{1 + m^2} \right) \end{array} \right)}, \tag{30}$$

6. Numerical Scheme

The system with high nonlinearity comprising Equations (12)–(15) with the support of Equation (16) is numerically solved by `bvp4c` MATLAB function. The following code transforms the given model into the 1st order system of ODEs.

$$\begin{aligned} g &= y_1, \\ g' &= y_2, \\ g'' &= y_3, \\ g''' &= y y_1, \\ y y_1 &= \frac{1}{2\xi} \left[\begin{array}{l} \lambda y_2 - 2y_3 + (1 - \phi)^{2.5} (1 - \phi + \phi \frac{\rho_{CNT}}{\rho_{bf}}) F_r y_2^2 \\ -(1 - \phi)^{2.5} \alpha \beta (y_5 - y_2) - (1 - \phi_d)(1 - \phi)^{2.5} (1 - \phi + \phi \frac{\rho_{CNT}}{\rho_{bf}}) y_1 y_3 \\ + (1 - \phi)^{2.5} \frac{M}{1 + m^2} y_2 \end{array} \right], \end{aligned} \tag{31}$$

$$\begin{aligned} \theta &= y_6, \\ \theta' &= y_7, \\ \theta'' &= y y_3, \end{aligned} \tag{32}$$

$$y y_3 = \frac{1}{\frac{k_{nf}}{k_{bf}} \xi + \frac{4}{3N_r} (1 + (\theta_r - 1)\theta)^3} \left[\begin{array}{l} \frac{k_{bf}}{k_{nf}} y_7 - 0.5Pr(1 - \phi)^{2.5} (1 - \phi + \phi \frac{\rho_{CNT}}{\rho_{bf}}) y_1 y_7 \\ - \frac{4}{N_r} (1 + (\theta_r - 1)\theta)^2 \xi (\theta_r - 1) \theta r^2 \\ - \frac{4}{3N_r} (1 + (\theta_r - 1)\theta)^3 0.5\theta' - \frac{4EcPr}{(1 - \phi)^{2.5}} \xi y_3^2 \\ - 2\alpha \beta EcPr (y_5 - y_2)^2 - 2EcPr \left(\frac{\lambda}{(1 - \phi)^{2.5}} + \frac{M}{1 + m^2} \right) y_2^2 \\ - 0.5\alpha \beta_T Pr (1 - \phi + \phi \frac{(C_p)_{CNT}}{(C_p)_{bf}}) (y_8 - y_6) \end{array} \right] \tag{33}$$

$$\begin{aligned}
 \theta_p &= y_8, \\
 \theta_{p,r} &= y y_4, \\
 y y_4 &= \frac{\gamma \beta_T (1 - \varphi + \varphi \frac{(C_p)_{CNT}}{(C_p)_{bf}})}{y_4} (y_8 - y_6).
 \end{aligned}
 \tag{34}$$

With boundary conditions

$$\begin{aligned}
 y_1(a) &= \frac{a}{2} \varepsilon, y_2(a) = \frac{\varepsilon}{2}, y_4(a) = \frac{a}{2} \varepsilon, y_5(a) = \frac{\varepsilon}{2}, \\
 y_6(a) &= 1, y_2(\infty) = 0, y_6(\infty) = 0, y_8(\infty) = 0.
 \end{aligned}
 \tag{35}$$

Table 3 depicts the validation of the obtained results by comparing with already published articles in limiting case. This endorses the truthfulness of the presented mathematical model.

Table 3. Validation of the existing model for the values of $g''(a)$ when $\varepsilon = \phi_d = \lambda = F_r = \alpha = \beta = M = m = 0$.

a	Ishak et al. [47]	Chen and Smith [42]	M. Idrees Afridi et al. [43]	Present Results
0.1	1.2888	1.28881	1.28881	1.28508
0.01	8.4924	8.49244	8.49233	8.4878
0.001	62.1637	62.16372	62.16370	62.1594

Table 4 illustrates the numerically calculated values of the skin friction coefficient for numerous estimates of $\alpha, \phi_d, F_r, \beta, M,$ and m . It is noticed that value of the drag force coefficient is higher for $\alpha, \phi_d, F_r,$ and $M,$ but it declines for estimates of β and m for both types of CNTs. Likewise, Table 5 portrays the Nusselt number for $F_r, \alpha, \beta, m, N_r,$ and θ_r . It is comprehended that heat transfer rate is higher in case of α and $F_r,$ but converse behavior is seen for $\beta, m, N_r,$ and θ_r for SWCNTs and MWCNTs.

Table 4. Skin friction coefficient against different parameters.

a	ϕ_d	F_r	β	M	m	Skin Friction Coefficient	
						SWCNT	MWCNT
0.001						0.00184647	0.00184157
0.01						0.00583012	0.00581468
0.2						0.02591430	0.02584880
	0.1					0.00583012	0.00581468
	2.0					0.00583276	0.00581722
	3.5					0.00583491	0.00581927
		0.10				0.00583012	0.00581468
		0.25				0.00644651	0.00640784
		0.4				0.00706302	0.00700110
			1.0			0.00583012	0.00581468
			2.0			0.00582586	0.00581043
			3.0			0.00582165	0.00580623
				0.2		0.00583012	0.00581468
				0.3		0.00711701	0.00710157
				0.4		0.00840431	0.00838888
					1.0	0.00583012	0.00581468
					1.4	0.00499559	0.00498015
					1.8	0.00447082	0.00445537

Table 5. Numerical values of Nusselt number against different parameters.

F_r	α	β	m	N_r	θ_r	Nusselt Number	
						SWCNT	MWCNT
0.10						1.10739	1.05489
0.25						1.12048	1.06695
0.40						1.13570	1.08087
	1.0					1.10739	1.05489
	2.0					1.28855	1.22836
	3.0					1.44647	1.37965
		0.3				1.12089	1.06788
		0.5				1.10739	1.05489
		0.9				1.09958	1.04738
			1.0			1.10739	1.05489
			1.4			1.09857	1.04640
			1.8			1.09329	1.04131
				6.0		1.10739	1.05489
				9.0		0.80951	0.77264
				15.0		0.59158	0.56589
					1.1	1.10739	1.05489
					1.4	0.80635	0.77013
					1.7	0.71356	0.68292

7. Results and Discussion

This segment was devoted to envisioning the physical insight for graphical illustration Figures 2–10. We took the fixed values of the parameters throughout the study as ($\alpha = 0.01$, $\varepsilon = 0.3$, $\phi = 0.04$, $\phi_d = F_r = \lambda = Ec = 0.1$, $\alpha = m = \gamma = 1$, $\beta = \beta_T = 0.5$, $M = 0.2$, $N_r = 6$, $\theta_r = 1.1$) and $Pr = 6.8$. Figure 2a,b exemplify the impacts of needle's size " a " on the nanofluid velocity and velocity of the dust phase, respectively. It was comprehended that velocities were declining functions of the needle size in the case of CNTs of both types. Physically speaking, both velocities were highly dependent on the size of the needle. Increasing the needle's size lowered the velocities, which was obvious. An opposite trend was witnessed in the case of Figure 2c,d. It was witnessed that temperature was dominant in the case of SWCNTs as compared to MWCNTs. This was because MWCNTs have lower thermal conductivity than SWCNTs.

The impact of radiation parameter N_r on the nanofluid temperature and temperature of the dust phase could be seen in Figure 3a,b. Owing to higher radiation, more heat was transmitted to both nanofluid and the dust phase. Eventually, the augmented temperature in both cases, i.e., nanofluid and dust fluid, was witnessed.

Variation in temperature ratio parameter θ_r on temperatures of the nanofluid and dust fluid is depicted in Figure 4a,b, respectively. θ_r is the quotient of the wall temperature to ambient temperature. Larger values of θ_r meant sturdier wall temperature than the ambient temperature. Higher estimates of θ_r resulted in a rise in the temperature of both fluids in the case of both CNTs.

Figure 5a,b revealed the nanofluid velocity and dust phase for the Darcy–Forchheimer parameter F_r . It is learned that both velocity functions are diminishing for the growing values of F_r [29]. Actually, higher estimates of F_r produced resistance in nanofluid motion for both CNTs that ultimately dropped nanofluid and dust fluid velocities.

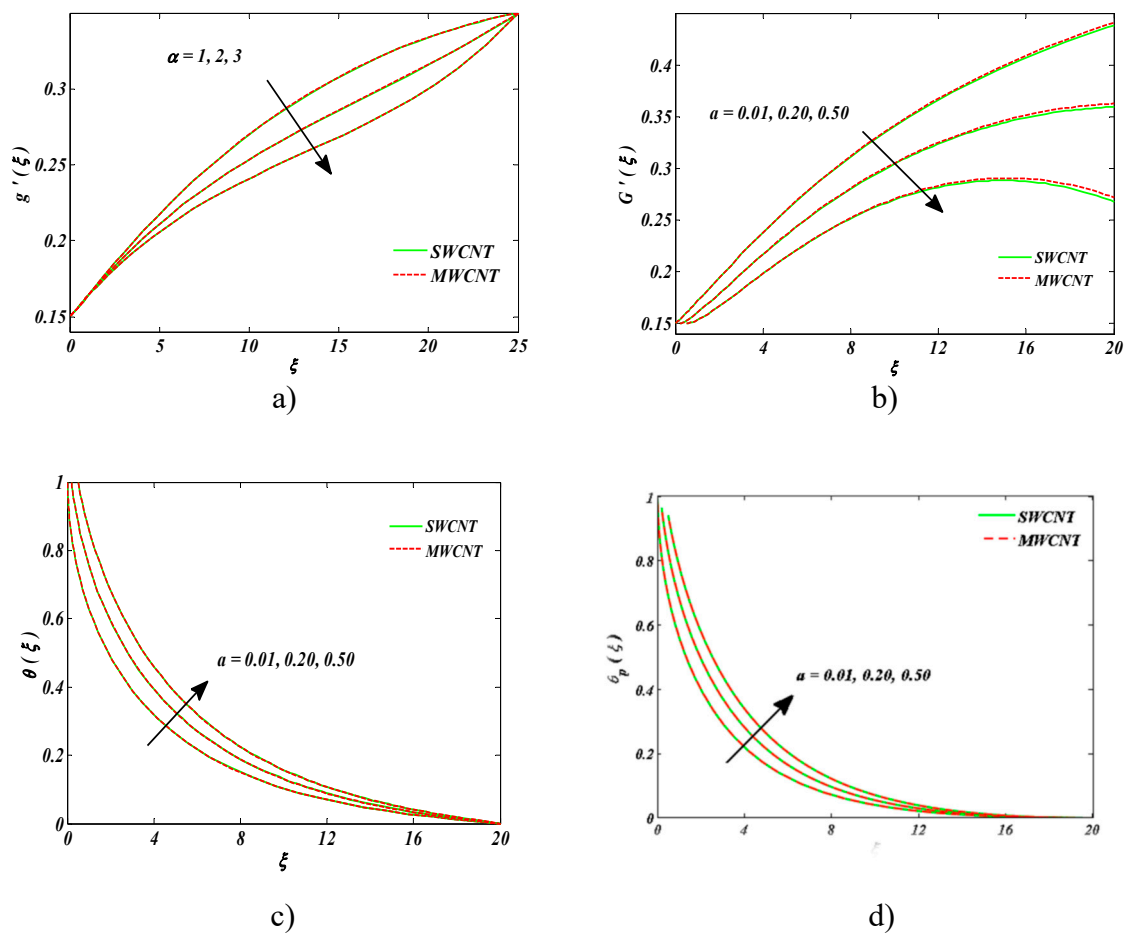


Figure 2. Impact of a on (a) nanofluid velocity, (b) the velocity of the dust phase, (c) nanofluid temperature, and (d) temperature of the dust phase.

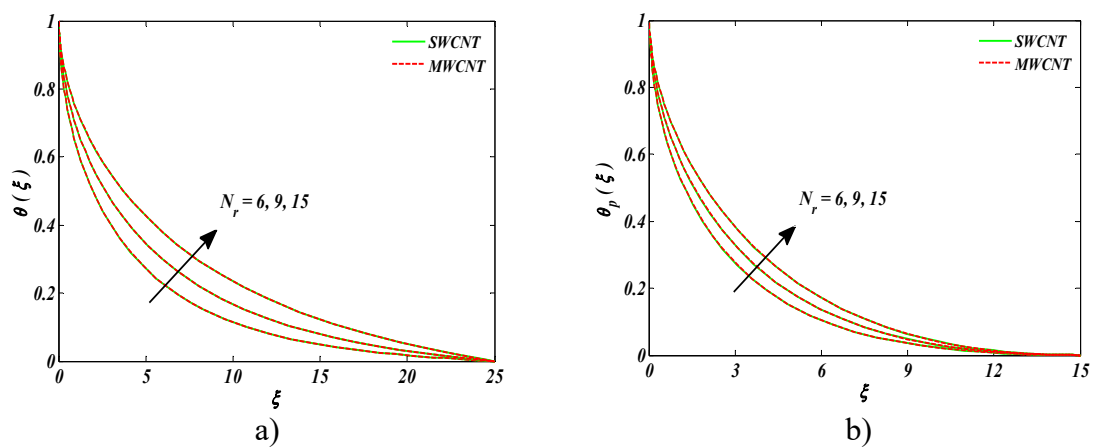


Figure 3. Impact of N_r on (a) nanofluid temperature and (b) temperature of the dust phase.

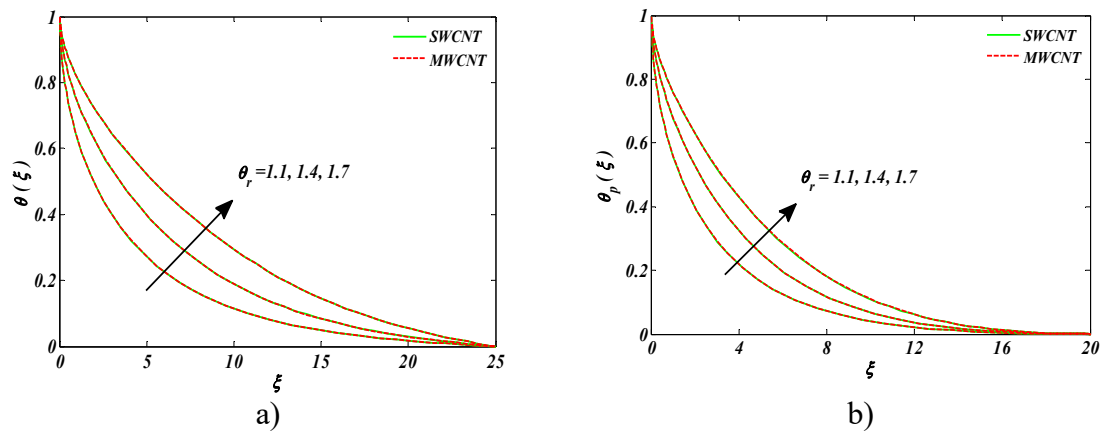


Figure 4. Impact of θ_r on (a) nanofluid temperature and (b) temperature of the dust phase.

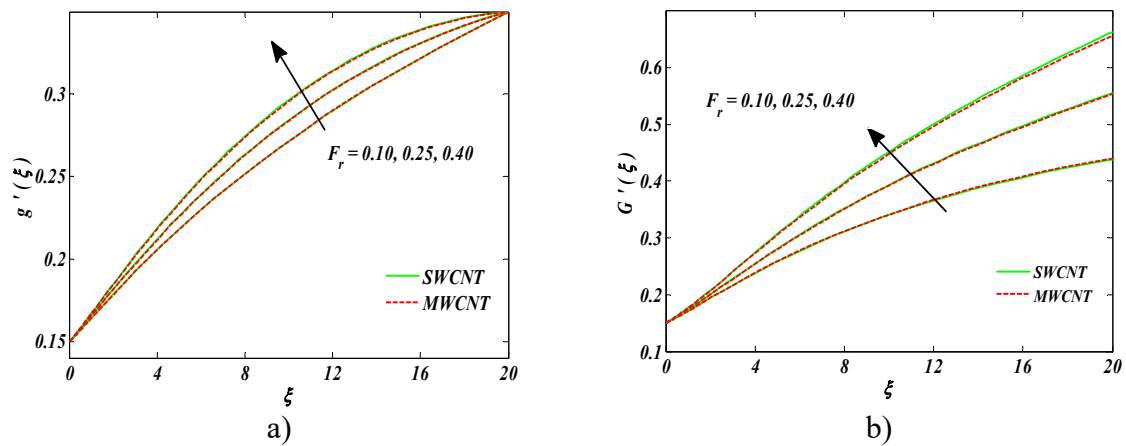


Figure 5. Impact of F_r on (a) nanofluid velocity and (b) the velocity of the dust phase.

The upshot of magnetic parameter M on associated distributions is described in Figure 6a–d. Upon increasing the number of dust particles into the fluid, the drag force was strengthened, and more resistance to the fluid flow was experienced, and, eventually, a decrease in both velocities was witnessed. An opposing trend was identified for the temperature field and the dust fluid temperature, which was obviously owing to sturdier M .

Figure 7a,b are outlined to perceive the impact of Hall current parameter m on both velocities. It was detected that velocities were mounting functions of m . Larger estimates of m enforced the damping force, and, eventually, velocities were strengthened.

The impression of Hall current m on entropy generation and the Bejan number is shown in Figure 8a,b. Larger values of m lowered the temperature that resulted in a drop of entropy generation as well. An inverse behavior was seen for the Bejan number against m .

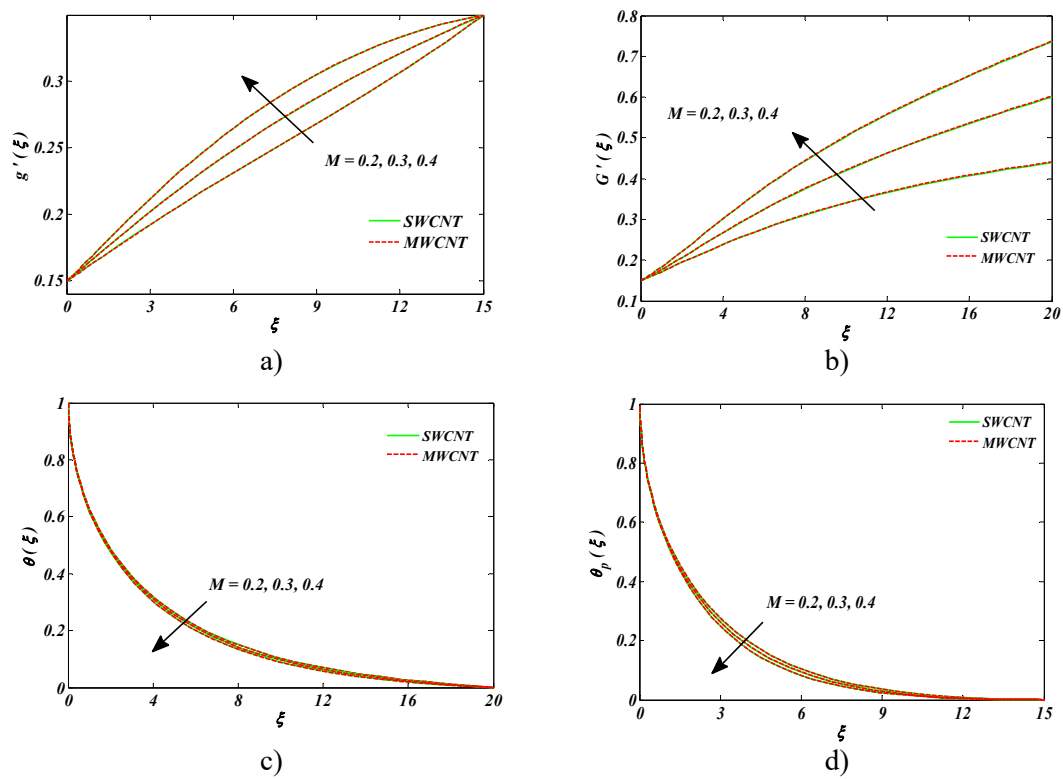


Figure 6. Impact of M on (a) nanofluid velocity, (b) the velocity of the dust phase, (c) nanofluid temperature, and (d) temperature of the dust phase.

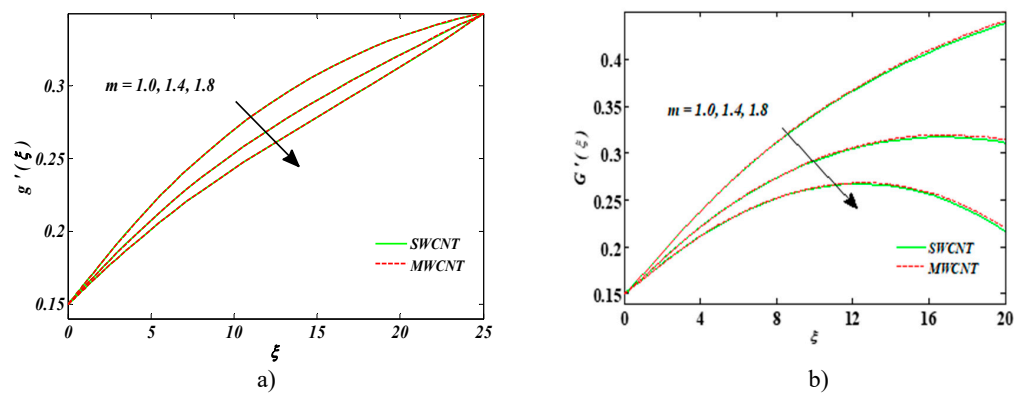


Figure 7. Impact of m on (a) nanofluid velocity and (b) the velocity of the dust phase.

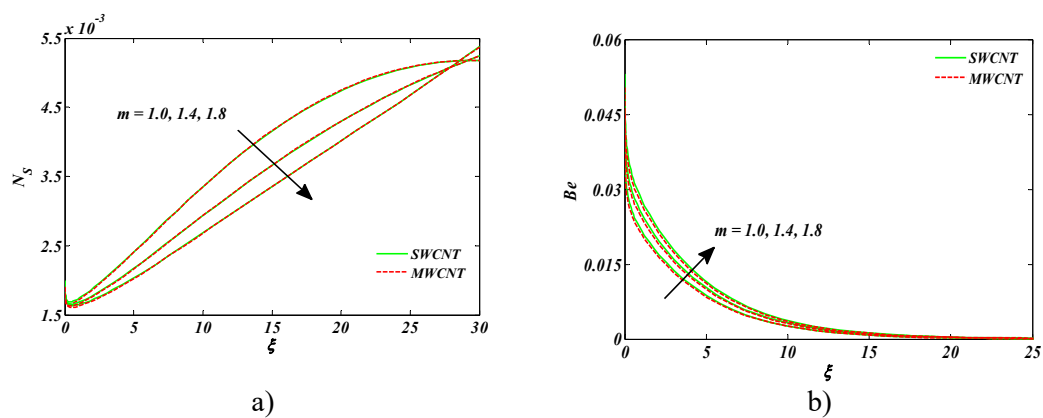


Figure 8. Impact of m on (a) entropy generation number and (b) Bejan number.

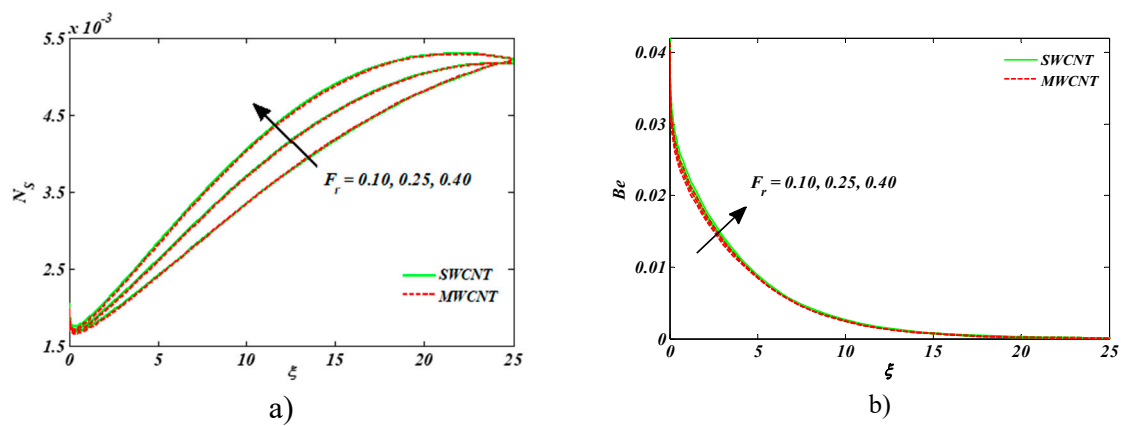


Figure 9. Impact of F_r on (a) entropy generation number and (b) Bejan number.

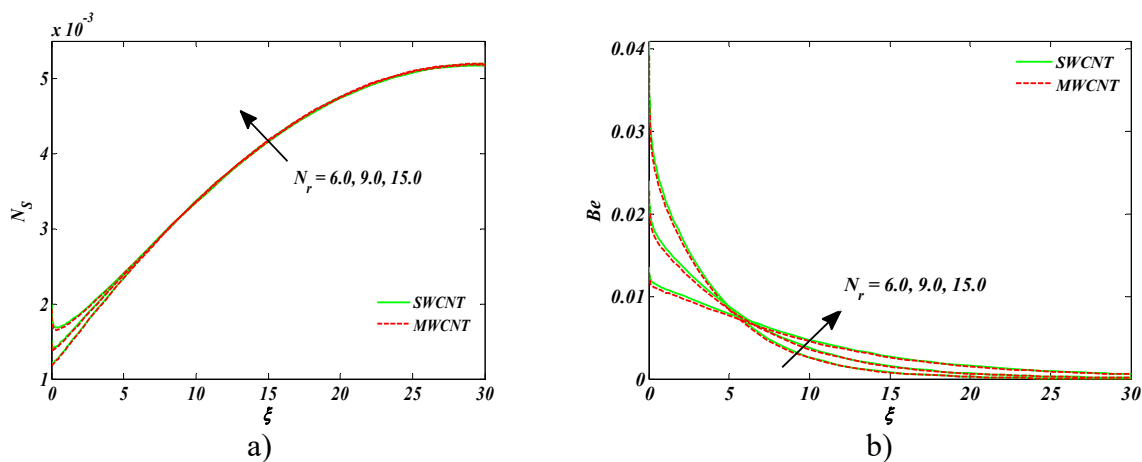


Figure 10. Impact of N_r on (a) entropy generation number and (b) Bejan number.

Figure 9a,b is plotted for entropy generation and Bejan number for Forchheimer parameter F_r . An upsurge was visualized in both cases. Larger estimates of the inertial coefficient boosted the disorderliness and caused it to intensify N_s and Be .

Figure 10a,b is sketched to comprehend the upshot of radiation parameter N_r on entropy generation and the Bejan number, respectively. An enhancement in both entropy generation and the Bejan number was witnessed versus the radiation parameter. This was all because of the heightened energy systems, owing to larger estimates of N_r .

8. Final Remarks

In the present exploration, Hall current sequel on the Darcy–Forchheimer H_2O -CNTs dusty nanofluid solution over a thin needle was investigated numerically. The novelty impacts of nonlinear thermal radiation with other effects were accompanied by entropy analysis. The leading outcomes of the investigation are appended as follows:

- Bejan number increased for larger values of Darcy–Forchheimer number.
- Velocity was on the decline once the size of the needle and Darcy–Forchheimer parameter’s values were enhanced.
- Higher estimates of Hall current parameter escalated the velocity profiles for both CNTs.
- An upsurge in entropy generation and the Bejan number was witnessed versus the radiation parameter.
- Sturdier magnetic field diminished the velocity of the fluid.
- Skin friction coefficient declined for growing estimates of dust particles’ mass concentration.

Author Contributions: Methodology, I.T.; Conceptualization, Project Administration, Writing—Original Draft, M.R.; Software, S.K.; Validation, H.-W.K.; Funding Acquisition, Writing—review and Editing, Y.N. All authors have read and agreed to the published version of the manuscript.

Funding: This research was supported by the Bio & Medical Technology Development Program of the NRF funded by the Korean government, MSIP(NRF-2015M3A9D7067219) and also supported by the Soonchunhyang University Research Fund.

Conflicts of Interest: The authors declare no conflict of interest.

Nomenclature

r	Coordinate measured in radial direction
(u, v)	Velocity components along x and r directions
μ_{nf}	Effective dynamic viscosity of nanofluid
ρ_{nf}	Density of nanofluid
ν_{nf}	Kinematic viscosity of nanofluid
k^*	Darcy-permeability of the porous medium
C_b	Drag coefficient
ϕ_d	Volume fraction of dust particles
K	Stokes resistance
N	Number density of dust particles
σ	Electric conductivity
B_0	Applied magnetic field
m	Hall parameter
m_d	Mass concentration of the dust particles
k_{nf}	Effective thermal conductivity of the nanofluid
$(\rho C_p)_{nf}$	Effective heat capacitance of the nanofluid
N_1	Density of the particle phase
τ_v	Relaxation time of dust particles
τ_T	Thermal equilibrium time
τ_w	Shear stress at the surface
\dot{S}'''_{GEN}	Entropy generation rate per unit volume
(u_p, v_p)	Velocity components of particle phase in x and r directions
c_m	Specific heat of the dust particles
u_w	Velocity of the moving needle
u_∞	Velocity outside the boundary layer
T	Dimensional temperature of the nanofluid
T_p	Temperature of the dust particle
T_w	Constant surface temperature of the thin needle
T_∞	Ambient temperature
λ	Porosity parameter
F_r	Forchheimer parameter
α	Dust particles mass concentration
β	Fluid particle interaction parameter for velocity
M	Magnetic field parameter
Pr	Prandtl number
N_r	Nonlinear radiation parameter
θ_r	Temperature ratio parameter
Ec	Eckert number
β_T	Fluid particle interaction parameter for temperature
γ	Ratio of specific heat
q_w	Surface heat flux
N_S	Entropy generation number

References

1. Bejan, A. A study of entropy generation in fundamental convective heat transfer. *J. Heat Transf.* **1979**, *101*, 718–725. [[CrossRef](#)]
2. Rehman, A.U.; Mehmood, R.; Nadeem, S. Entropy analysis of radioactive rotating nanofluid with thermal slip. *Appl. Therm. Eng.* **2017**, *112*, 832–840. [[CrossRef](#)]
3. Zeeshan, A.; Shehzad, N.; Abbas, T.; Ellahi, R. Effects of radiative electro-magnetohydrodynamics diminishing internal energy of pressure-driven flow of titanium dioxide-water nanofluid due to entropy generation. *Entropy* **2019**, *21*, 236. [[CrossRef](#)]
4. Lu, D.; Ramzan, M.; Mohammad, M.; Howari, F.; Chung, J.D. A Thin Film Flow of Nanofluid Comprising Carbon Nanotubes Influenced by Cattaneo-Christov Heat Flux and Entropy Generation. *Coatings* **2019**, *9*, 296. [[CrossRef](#)]
5. Hassan, M.; Mohyud-Din, S.T.; Ramzan, M. Study of heat transfer and entropy generation in ferrofluid under low oscillating magnetic field. *Indian J. Phys.* **2019**, *93*, 749–758. [[CrossRef](#)]
6. Suleman, M.; Ramzan, M.; Zulfikar, M.; Bilal, M.; Shafee, A.; Chung, J.D.; Lu, D.; Farooq, U. Entropy analysis of 3D non-Newtonian MHD nanofluid flow with nonlinear thermal radiation past over exponential stretched surface. *Entropy* **2018**, *20*, 930. [[CrossRef](#)]
7. Ramzan, M.; Sheikholeslami, M.; Chung, J.D.; Shafee, A. Melting heat transfer and entropy optimization owing to carbon nanotubes suspended Casson nanoliquid flow past a swirling cylinder—A numerical treatment. *AIP Adv.* **2018**, *8*, 115130. [[CrossRef](#)]
8. Li, Z.; Hedayat, M.; Sheikholeslami, M.; Shafee, A.; Zrelli, H.; Tlili, I.; Nguyen, T.K. Numerical simulation for entropy generation and hydrothermal performance of nanomaterial inside a porous cavity using Fe₃O₄ nanoparticles. *Phys. A* **2019**, *524*, 272–288. [[CrossRef](#)]
9. Khan, M.I.; Shah, F.; Hayat, T.; Alsaedi, A. Transportation of CNTs based nanomaterial flow confined between two coaxially rotating disks with entropy generation. *Phys. A* **2019**, *527*, 121154. [[CrossRef](#)]
10. Abbas, S.Z.; Khan, W.A.; Sun, H.; Ali, M.; Irfan, M.; Shahzed, M.; Sultan, F. Mathematical modeling and analysis of Cross nanofluid flow subjected to entropy generation. *Appl. Nanosci.* **2019**, 1–2. [[CrossRef](#)]
11. Iijima, S. Helical microtubules of graphitic carbon. *Nature* **1991**, *354*, 56. [[CrossRef](#)]
12. Bethune, D.S.; Kiang, C.H.; De Vries, M.S.; Gorman, G.; Savoy, R.; Vazquez, J.; Beyers, R. Cobalt-catalysed growth of carbon nanotubes with single-atomic-layer walls. *Nature* **1993**, *363*, 605. [[CrossRef](#)]
13. Baughman, R.H.; Zakhidov, A.A.; De Heer, W.A. Carbon nanotubes—the route toward applications. *Science* **2002**, *297*, 787–792. [[CrossRef](#)] [[PubMed](#)]
14. Dresselhaus, M.S.; Dresselhaus, G.; Eklund, P.C. *Science of Fullerenes and Carbon Nanotubes: Their Properties and Applications*; ACADEMIC PRESS: New Yourk, NY, USA, 1996.
15. De Volder, M.F.; Tawfick, S.H.; Baughman, R.H.; Hart, A.J. Carbon nanotubes: Present and future commercial applications. *Science* **2013**, *339*, 535–539. [[CrossRef](#)]
16. Chamkha, A.J.; Abbasbandy, S.; Rashad, A.M.; Vajravelu, K. Radiation effects on mixed convection about a cone embedded in a porous medium filled with a nanofluid. *Meccanica* **2013**, *48*, 275–285. [[CrossRef](#)]
17. Choi, S.U.; Eastman, J.A. *Enhancing Thermal Conductivity of Fluids with Nanoparticles*; Argonne National Lab: Du Page County, IL, USA, 1995.
18. Eastman, J.A.; Choi, U.S.; Li, S.; Thompson, L.J.; Lee, S. Enhanced thermal conductivity through the development of nanofluids. *MRS Online Proc. Libr. Arch.* **1996**. [[CrossRef](#)]
19. Keblinski, P.; Phillpot, S.R.; Choi, S.U.; Eastman, J.A. Mechanisms of heat flow in suspensions of nano-sized particles (nanofluids). *Int. J. Heat Mass Transf.* **2002**, *45*, 855–863. [[CrossRef](#)]
20. Makinde, O.D.; Aziz, A. Boundary layer flow of a nanofluid past a stretching sheet with a convective boundary condition. *Int. J. Therm. Sci.* **2011**, *50*, 1326–1332. [[CrossRef](#)]
21. Sheikholeslami, M.; Shehzad, S.A. Numerical analysis of Fe₃O₄–H₂O nanofluid flow in permeable media under the effect of external magnetic source. *Int. J. Heat Mass Transf.* **2018**, *118*, 182–192. [[CrossRef](#)]
22. Khan, M.I.; Kumar, A.; Hayat, T.; Waqas, M.; Singh, R. Entropy generation in flow of Carreau nanofluid. *J. Mol. Liq.* **2019**, *278*, 677–687. [[CrossRef](#)]
23. Sheikholeslami, M. New computational approach for exergy and entropy analysis of nanofluid under the impact of Lorentz force through a porous media. *Comput. Method Appl. M* **2019**, *344*, 319–333. [[CrossRef](#)]

24. Khan, W.A.; Sultan, F.; Ali, M.; Shahzad, M.; Khan, M.; Irfan, M. Consequences of activation energy and binary chemical reaction for 3D flow of Cross-nanofluid with radiative heat transfer. *J. Braz. Soc. Mech. Sci.* **2019**, *41*, 4. [[CrossRef](#)]
25. Hosseini, S.R.; Sheikholeslami, M. Investigation of the nanofluid convective flow and entropy generation within a microchannel heat sink involving magnetic field. *Powder Technol.* **2019**, *351*, 195–202. [[CrossRef](#)]
26. Ahmed, J.; Khan, M.; Ahmad, L. MHD swirling flow and heat transfer in Maxwell fluid driven by two coaxially rotating disks with variable thermal conductivity. *Chin. J. Phys.* **2019**, *60*, 22–34. [[CrossRef](#)]
27. Cheng, B.; Yang, S.; Liu, H.; Zhang, L.; Wang, F. Investigation of the interaction between carbon nanotube tip and silicon sample through molecular dynamic simulation. *Chin. J. Phys.* **2019**, *60*, 407–415. [[CrossRef](#)]
28. Talla, J.A.; Alsaliyby, A.F. Effect of uniaxial tensile strength on the electrical properties of doped carbon nanotubes: Density functional theory. *Chin. J. Phys.* **2019**, *59*, 418–425. [[CrossRef](#)]
29. Bilal, M.; Ramzan, M. Hall current effect on unsteady rotational flow of carbon nanotubes with dust particles and nonlinear thermal radiation in Darcy–Forchheimer porous media. *J. Therm. Anal. Calorim.* **2019**, *138*, 3127–3137. [[CrossRef](#)]
30. Nadeem, S.; Abbas, N.; Elmasry, Y.; Malik, M.Y. Numerical analysis of water based CNTs flow of micropolar fluid through rotating frame. *Comput. Methods Programs Biomed.* **2020**, *186*, 105194. [[CrossRef](#)]
31. Ibrahim, M.; Khan, M.I. Mathematical modeling and analysis of SWCNT-Water and MWCNT-Water flow over a stretchable sheet. *Comput. Methods Programs Biomed.* **2019**, *187*, 105222. [[CrossRef](#)]
32. Shahzadi, I.; Sadaf, H.; Nadeem, S.; Saleem, A. Bio-mathematical analysis for the peristaltic flow of single wall carbon nanotubes under the impact of variable viscosity and wall properties. *Comput. Methods Programs Biomed.* **2017**, *139*, 137–147. [[CrossRef](#)]
33. Maleki, R.; Afrouzi, H.H.; Hosseini, M.; Toghraie, D.; Piranfar, A.; Rostami, S. pH-sensitive loading/releasing of doxorubicin using single-walled carbon nanotube and multi-walled carbon nanotube: A molecular dynamics study. *Comput. Methods Programs Biomed.* **2020**, *186*, 105210. [[CrossRef](#)]
34. Zheng, S.; Liang, W.; Chu, H.; Zhou, H. Effects of radiation reabsorption of C₁–C₆ hydrocarbon flames at normal and elevated pressures. *Fuel* **2020**, *266*, 117061. [[CrossRef](#)]
35. Khan, M.I.; Qayyum, S.; Hayat, T.; Waqas, M.; Khan, M.I.; Alsaedi, A. Entropy generation minimization and binary chemical reaction with Arrhenius activation energy in MHD radiative flow of nanomaterial. *J. Mol. Liq.* **2018**, *259*, 274–283. [[CrossRef](#)]
36. Ramzan, M.; Mohammad, M.; Howari, F.; Chung, J.D. Entropy analysis of carbon nanotubes based nanofluid flow past a vertical cone with thermal radiation. *Entropy* **2019**, *21*, 642. [[CrossRef](#)]
37. Sheikholeslami, M.; Behnoush, R.; Milad, D.; Ahmad, S.; Zhixiong, Li.; Truong, K.N. Application of nano-refrigerant for boiling heat transfer enhancement employing an experimental study. *Int. J. Heat Mass Transfer.* **2019**, *141*, 974–980. [[CrossRef](#)]
38. Ramzan, M.; Riasat, S.; Kadry, S.; Long, C.; Nam, Y.; Lu, D. Numerical simulation of 3D condensation nanofluid film flow with Carbon nanotubes on an inclined rotating disk. *Appl. Sci.* **2020**, *10*, 168. [[CrossRef](#)]
39. Ramzan, M.; Mohammad, M.; Howari, F. Magnetized suspended carbon nanotubes based nanofluid flow with bio-convection and entropy generation past a vertical cone. *Sci. Rep.* **2019**, *9*, 1–5. [[CrossRef](#)]
40. Karvelas, E.; Liosis, C.; Benos, L.; Karakasidis, T.; Sarris, I. Micromixing efficiency of particles in heavy metal removal processes under various inlet conditions. *Water.* **2019**, *11*, 1135. [[CrossRef](#)]
41. Fragkou, A.D.; Karakasidis, T.E.; Sarris, I.E. Recurrence quantification analysis of MHD turbulent channel flow. *Phys. A Stat. Mech. Appl.* **2019**, *531*, 121741. [[CrossRef](#)]
42. Chen, J.L.; Smith, T.N. Forced convection heat transfer from nonisothermal thin needles. *J. Heat Transf.* **1978**, *100*, 358–362. [[CrossRef](#)]
43. Afridi, M.I.; Tlili, I.; Qasim, M.; Khan, I. Nonlinear Rosseland thermal radiation and energy dissipation effects on entropy generation in CNTs suspended nanofluids flow over a thin needle. *Bound Value Probl.* **2018**, *2018*, 148. [[CrossRef](#)]
44. Sulochana, C.; Prakash, J.; Sandeep, N. Unsteady MHD flow of a dusty nanofluid past a vertical stretching surface with non-uniform heat source/sink. *Int. J. Sci. Eng.* **2016**, *10*, 1–9.
45. Raju, C.S.; Saleem, S.; Al-Qarni, M.M.; Upadhya, S.M. Unsteady nonlinear convection on Eyring–Powell radiated flow with suspended graphene and dust particles. *Microsyst. Technol.* **2019**, *25*, 1321–1331. [[CrossRef](#)]

46. Xue, Q.Z. Model for thermal conductivity of carbon nanotube-based composites. *Phys. B* **2005**, *368*, 302–307. [[CrossRef](#)]
47. Ishak, A.; Nazar, R.; Pop, I. Boundary layer flow over a continuously moving thin needle in a parallel free stream. *Chin. Phys. Lett.* **2007**, *24*, 2895. [[CrossRef](#)]



© 2020 by the authors. Licensee MDPI, Basel, Switzerland. This article is an open access article distributed under the terms and conditions of the Creative Commons Attribution (CC BY) license (<http://creativecommons.org/licenses/by/4.0/>).